applied sciences

MDPI

Article

Effects of Target Material Properties on Acceleration Characteristics During Sequential Multiple-Target Impacts Based on Quantitative Prediction Models

Huifa Shi [1], Feiyin Li [2], Kunming Jia [1], Shaojie Ma [1,*] and Xinping Zhang [3]

[1] School of Mechanical Engineering, Nanjing University of Science and Technology, Nanjing 210094, China; shihf@njust.edu.cn (H.S.); kunming_jia@163.com (K.J.)
[2] School of Locomotive and Rolling Stock, Nanjing Vocational Institute of Railway Technology, Nanjing 210031, China; feiyinli@njrts.edu.cn
[3] School of Material Science and Engineering, Nanjing University of Science and Technology, Nanjing 210094, China; xpzhang@njust.edu.cn
* Correspondence: shaojiem@njust.edu.cn

Abstract

To address the damage and failure of electromechanical structures such as Printed Circuit Board (PCB) modules and battery assemblies under multiple impacts, this study combined experimental and modeling approaches to quantitatively investigate the influence of target material mechanical properties on impact acceleration characteristics. Quasi-static tensile/compression tests, split-Hopkinson pressure bar dynamic compression tests, and sequential multiple-target impact experiments were conducted on nine metallic materials, providing constitutive parameters and impact response data. Variance analysis revealed that material type significantly affected acceleration characteristics ($p \leq 1.62 \times 10^{-5}$), whereas the target position in the impact sequence was statistically insignificant ($p \geq 0.89$). Quantitative prediction models were established for different acceleration characteristics: Ridge regression ($\alpha = 0.1$) was employed for Peak 1–Peak 3, Duration 1, and Duration 3, while linear regression was used for Duration 2. The results quantitatively demonstrated that the elastic modulus was positively associated with both peak acceleration and duration, while dynamic compressive yield strength exhibited a significant negative influence. This work establishes a preliminary quantitative predictive framework that provides guidance for target material selection in sequential multiple-target impact experiments and offers an experimental approach for generating tunable overload responses in high-intensity impact testing of electromechanical components.

Keywords: mechanical properties; target; acceleration characteristics; predictive model; sequential multiple-target impacts

Academic Editor: Ana Martins Amaro

Received: 11 May 2026
Revised: 29 May 2026
Accepted: 3 June 2026
Published: 5 June 2026

1. Introduction

The dynamic responses and functional reliability of electromechanical structures, such as printed circuit board (PCB) modules, battery systems, and other electromechanical components, under impact loading are important issues in the safety assessment of aerospace systems, defense equipment, transportation systems, and high-reliability electronic devices [1]. These structures may be subjected to single or multiple impact loads in typical service scenarios, such as automotive collisions, aircraft landings, and missile penetration processes [2–4]. Such loads are generally characterized by short durations

and high acceleration amplitudes. When the acceleration amplitude or pulse duration exceeds the load-bearing capacity of the structure, damage such as fatigue crack propagation at solder-joint interfaces and package cracking may be induced, eventually leading to functional failure of the electromechanical structure [5,6]. Therefore, quantitative evaluation and prediction methods for impact acceleration characteristics should be established to guide controlled multiple-impact testing before service and improve the reliability of electromechanical components under complex impact conditions [7,8].

Existing studies on impact responses and their influencing factors have mainly employed experimental testing, theoretical/numerical analysis, and data-driven modeling. In terms of experimental testing, drop-weight impact tests [9], air-gun impact tests [10], split-Hopkinson pressure bar (SHPB) high-strain-rate tests [11,12], and sequential multiple-target impact tests [13] have commonly been used to investigate structural impact responses, dynamic mechanical properties of materials, and multiple-impact loading characteristics. In theoretical and numerical analyses, contact mechanics, stress-wave theory, energy-balance analysis, and finite element simulations have been used to reveal the effects of impact duration, boundary conditions, wave propagation, plastic deformation, and fracture behavior on impact responses. In recent years, regression models, regularized regression methods, and data-driven surrogate models have also been increasingly used to establish mapping relationships among material parameters, structural parameters, and impact responses, thereby improving the efficiency of impact-response prediction and parameter design [14]. These experimental, theoretical, and data-driven methods provide an important basis for impact-response analysis and offer methodological support for further investigating the effects of target material parameters on acceleration characteristics under sequential multiple-target impacts.

Most existing studies on the factors affecting impact loading have focused on single-impact or single-target penetration conditions, and important progress has been made. Previous studies have shown that impact velocity, incident angle, impactor configuration, target plate structure, and target mechanical properties can affect impact loads and acceleration responses. In general, impact velocity is an important factor affecting peak load and peak acceleration [15–17]. The incident angle and impactor geometry can change the contact area and load-transfer path, and the maximum peak acceleration is usually obtained under normal impact at 90° [18–20]. Target thickness can affect penetration resistance and energy absorption, thereby changing the acceleration response [21]. These studies provide an important basis for understanding the formation mechanism of impact loads.

Among the factors reported in previous studies, target material parameters have also received considerable attention because of their influence on impact responses. The elastic modulus of the target material is generally related to contact stiffness and elastic stress-wave propagation, and a higher elastic modulus may lead to a higher instantaneous contact force and acceleration peak [21–24]. Yield strength and dynamic compressive yield strength reflect the resistance of a material to plastic deformation under quasi-static and high-strain-rate conditions, respectively, and may affect plastic energy dissipation, pulse duration, and peak response during impact [25]. Density, ductility, and strain-rate sensitivity may also influence the inertial effect, deformation mode, and energy absorption capacity of the target material [26]. Therefore, establishing the relationship between target material parameters and impact acceleration characteristics from the perspective of mechanical properties is important for target material selection and overload-response regulation in multiple-impact tests.

However, most existing studies have focused on single-impact, single-target penetration, or structural impact resistance, with emphasis mainly placed on penetration depth, damage modes, penetration resistance, and energy absorption characteristics. In sequential

multiple-target impacts, after the impactor completes its interaction with the previous target plate, its velocity, vibration state, stress-wave propagation state, and residual kinetic energy may change, which may further affect the contact state and load-transfer process at the subsequent target positions [27,28]. Therefore, the relationship between target material parameters and impact responses obtained under single-impact conditions cannot be directly extended to sequential multiple-target impact conditions. In particular, systematic experimental studies and quantitative prediction models are still lacking for clarifying how material parameters, such as elastic modulus and dynamic compressive yield strength, affect acceleration peaks and pulse durations at different target positions.

Therefore, systematic sequential multiple-target impact experiments were conducted in this study to investigate the effects of target material parameters on acceleration characteristics under multiple impacts. Nine metallic target materials with different stiffness, strength, density, and ductility were selected, and their mechanical properties were characterized through quasi-static tensile tests, quasi-static compression tests, and SHPB dynamic compression tests. Sequential multiple-target impact experiments were then performed, and acceleration characteristic parameters, including Peak 1–Peak 3 and Duration 1–Duration 3, were extracted to analyze the effects of material parameters, such as elastic modulus and dynamic compressive yield strength, on impact responses at different target positions. On this basis, preliminary quantitative prediction models correlating material parameters with impact acceleration responses were established using linear regression and regularized linear regression models, including Ridge regression, Lasso regression, and Elastic Net. The applicability of different models under small-sample and multivariable conditions was also compared. The results can provide guidance for target material selection in sequential multiple-target impact experiments and offer an experimental approach for generating tunable overload responses in high-intensity impact testing of electromechanical components.

The novelty of this study lies in combining quasi-static testing, SHPB dynamic compression testing, sequential multiple-target impact experiments, and regression modeling to quantify the material-dependent acceleration response under sequential multiple-target impact loading. The main contributions of this work are summarized as follows:

- Nine metallic target materials with different stiffness, strength, density, and ductility were selected, and their quasi-static and dynamic mechanical properties were systematically characterized;
- The relative influence of material mechanical properties and target position in the impact sequence on acceleration peaks and pulse durations was quantitatively evaluated;
- Preliminary quantitative prediction models were established for Peak 1–Peak 3 and Duration 1–Duration 3 based on material mechanical properties;
- A target-material selection strategy was proposed to provide guidance for sequential multiple-target impact experiments and for generating tunable overload responses in high-intensity impact testing of electromechanical components.

2. Materials and Experimental Methods

This section describes the target materials, mechanical property characterization methods, and sequential multiple-target impact experimental procedure used in this study. Nine metallic materials were selected to cover a wide range of stiffness, strength, and ductility. Their quasi-static and dynamic mechanical properties were first characterized and then used as input Variables for the subsequent quantitative prediction models. Sequential multiple-target impact experiments were further conducted to obtain acceleration peaks and pulse durations, which were used as output Variables in the models.

2.1. Target Materials

This study selects nine typical metallic materials as impact targets, including structural steels (AISI 1020/1040/1060), aluminum alloys (2A12/7020/7075), magnesium alloy (AZ31B), copper alloy (H62 brass), and stainless steel (S30153), to investigate the influence of material type and mechanical properties on sequential multiple-target impact responses. The selected materials were chosen to cover a wide and representative range of key mechanical properties—specifically elastic modulus, strength, density, and ductility—which have been identified in prior single-impact studies (as discussed in the Introduction) as significantly influencing impact load characteristics. For instance, the selected materials exhibit distinct elastic moduli that can be categorized into three broad groups: ~210 GPa (AISI 1020/1040/1060 steels and S30153 stainless steel), ~100 GPa (H62 brass), and 40–75 GPa (aluminum and magnesium alloys), ensuring significant inter-group variability. Similarly, their ultimate tensile strengths range from approximately 180 MPa (AZ31B) to over 690 MPa (AISI 1060 steel), and elongation varies from ~8.7% (AZ31B) to ~54.3% (S30153), providing a comprehensive spectrum of strength and ductility (as shown in Section 3.1. Mechanical properties of materials). The selected materials also exhibited different chemical compositions (Table 1), enabling a thorough characterization of mechanical response characteristics across different metallic systems.

Table 1. Chemical composition of experimental materials (wt.%).

Element	AISI 1020 Steel	AISI 1040 Steel	AISI 1060 Steel	2A12 Al Alloy	7020 Al Alloy	7075 Al Alloy	AZ31B Mg Alloy	H62 Brass	S30153 Stainless Steel
C	0.22	0.42	0.62	-	-	-	-	-	0.15
Si	0.2	0.3	0.183	0.04	0.12	0.23	0.0005	-	1
Mn	0.46	0.63	0.75	0.62	0.29	0.22	0.27	-	2
P	0.018	0.03	0.013	-	-	-	-	-	≤0.045
S	0.009	0.03	0.003	-	-	-	-	-	≤0.030
Ni	0.01	0.04	0.004	0.04	-	-	0.0002	-	6–8
Cr	0.04	0.04	0.16	-	0.22	0.24	-	-	16–18
Cu	0.02	0.05	0.006	4.71	0.02	1.65	0.0003	61.03	-
Fe	-	-	-	0.22	0.16	0.31	0.0006	0.031	-
Mg	-	-	-	1.52	1.32	2.36	-	-	-
Zn	-	-	-	0.04	4.6	5.72	0.57	Bal.	-
Al	-	-	-	Bal.	Bal.	Bal.	8.73	-	-
Be	-	-	-	-	-	-	0.0001	-	-
Pb	-	-	-	-	-	-	-	0.011	-
N	-	-	-	-	-	-	-	-	≤0.010

2.2. Quasi-Static Tensile and Compression Tests

Quasi-static mechanical property tests were conducted in strict accordance with GB/T 7314-2017 [29] and GB/T 228.1-2021 [30] standards using a Wance ETM105D universal testing machine (Shenzhen Wance Testing Machine Co., Ltd., Shenzhen, China). Standard tensile and compression specimens were used, and their geometries and dimensions were prepared according to the corresponding GB/T standards. The strain rate was controlled at 0.00067 s^{-1} for tensile tests and 0.001 s^{-1} for compression tests. Five mechanical parameters were systematically evaluated.

1. The elastic modulus, which was determined from the slope of the initial linear segment of the stress–strain curve;
2. The tensile yield strength;
3. The ultimate tensile strength;

4. The elongation percentage, which was calculated based on gauge length variation;
5. The compressive yield strength.

Strain measurements during tensile tests were performed using a Wance EX05005 extensometer. Three specimens were tested for each condition, and the average values were used for subsequent analysis and model construction.

2.3. SHPB Dynamic Compression Tests

A standard split-Hopkinson pressure bar (Figure 1) was employed for dynamic compression tests at a nominal strain rate of approximately 4000 s^{-1}. Because the nine metallic materials had different mechanical properties and wave impedances, the actual strain rates were not strictly identical for all specimens but varied within the range of 3802–4397 s^{-1}. One specimen was tested for each material under the dynamic compression tests. The testing system consisted of a gas gun-launched striker impacting a 2 m incident bar, with stress waves transmitted through a 1.5 m transmission bar. Both pressure bars exhibited identical material properties with a density of 7800 kg/m^3 and an elastic modulus of 210 GPa. The specimen was precisely positioned between the incident and transmission bars. Dynamic strain gauges coupled with data acquisition systems recorded the dynamic response, with particular emphasis on determining the material's dynamic yield compressive strength. An energy absorption device was incorporated to ensure experimental safety. This configuration satisfied all the requirements necessary to evaluate a material's mechanical properties under a high strain rate.

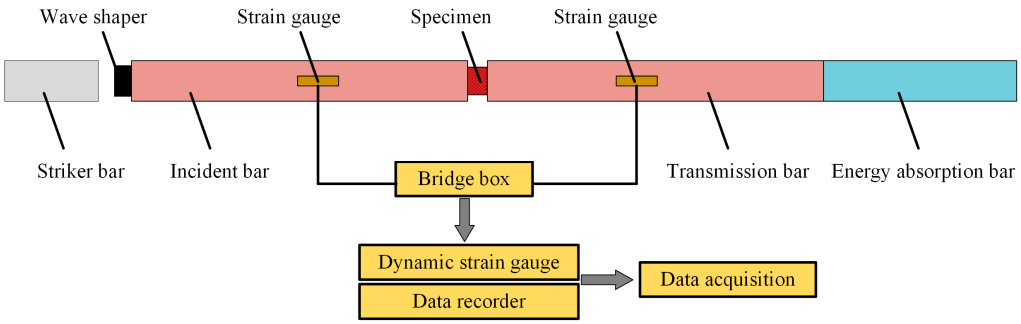

Figure 1. Schematic of the conventional split Hopkinson pressure bar apparatus.

During the test, the striker bar impacted the incident bar and generated an elastic stress wave. When the incident wave propagated to the specimen interface, it induced dynamic compressive deformation of the specimen. Owing to the impedance mismatch between the bars and the specimen, part of the incident wave was reflected back into the incident bar, while the remaining part was transmitted into the transmission bar.

The waveform data were acquired by strain gauges mounted on both bars. Analysis of transmitted and reflected wave signals based on one-dimensional stress wave theory was used to obtain the dynamic stress–strain response characteristics of specimens under a high strain rate. This method enabled the accurate determination of a material's dynamic mechanical properties.

The quasi-static and dynamic mechanical properties obtained in Sections 2.2 and 2.3 were then used as potential input Variables for the subsequent regression analysis of impact acceleration characteristics.

2.4. Sequential Multiple-Target Impact Experiments

Sequential multiple-target impact experiments were conducted using a rotational-arm impact testing apparatus (Figure 2) [13]. In this study, sequential multiple-target impacts refer to the successive interactions between the impactor and three independent target

plates in one experimental run. The impactor was fixed at the end of a rotational-arm with a length of 1 m and was driven at an angular velocity of 45 rad/s. The impactor had a frustum-cylinder structure, with a 20 mm diameter frustum top surface and a 60 mm diameter cylindrical base. During the experiment, the rotational-arm drove the impactor to successively impact and perforate three independent target plates.

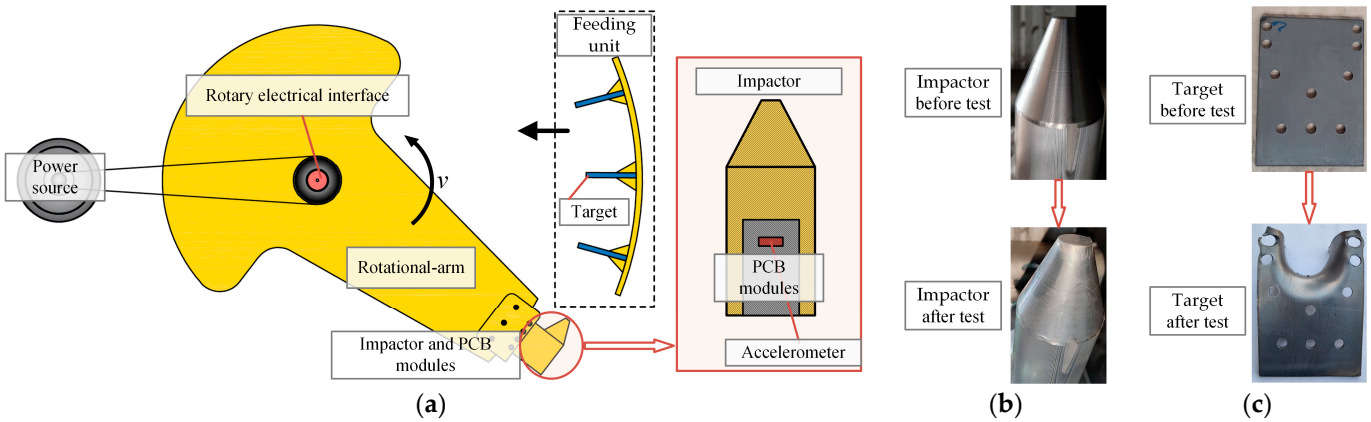

Figure 2. Rotational-arm impact testing apparatus: (**a**) Schematic diagram; (**b**) Impactor before and after impact; (**c**) Representative target plate before and after impact.

The three independent target plates were installed in the feeding unit of the rotational-arm impact testing apparatus and were fed into the predefined impact station as a target assembly before testing. The target plates were arranged successively along the impact path, allowing the impactor to interact with the first, second, and third plates in sequence during one experimental run. Each target plate had overall dimensions of 190 × 150 × 6 mm, and the spacing between adjacent target plates was 98 mm. The feeding unit was used to maintain the target alignment, impact position, and inter-plate spacing. The same target arrangement, feeding position, alignment condition, and impact parameters were maintained for all tested materials to ensure the consistency and comparability of the experimental results.

During each impact event, the interaction between the impactor and the target plate generated resistance, enabling measurable acceleration signals to be obtained from the PCB module with a diameter of 40 mm. The PCB module consisted of a high-precision accelerometer encapsulated in a potted metallic housing. This configuration ensured structural integrity and reliable signal acquisition under high-intensity impact loading. The metallic housing was fixed to the impactor, allowing the acceleration response of the impactor during the sequential multiple-target impacts to be measured.

An integrated measurement system was employed to acquire data during the sequential multiple-target impact experiments. The high-precision accelerometer embedded in the PCB module was fixed together with the impactor and rotated with the rotational-arm during testing. Therefore, a rotary electrical interface was used to transmit the accelerometer output signal from the rotating part to the data acquisition device (Figure 2a). The accelerometer and the data acquisition device were powered by a regulated constant-voltage power supply to ensure stable circuit operation and reduce electrical interference. Through this measurement system, the acceleration time-history signals of the impactor during successive interactions with the three independent target plates were recorded reliably.

For each material, three independent experimental runs were conducted to assess repeatability. In each run, the impactor successively interacted with three independent target plates made of the same material, and each target plate was impacted only once. Each target plate was an independent structure, and the perforation of one target plate

was completed before the impactor contacted the next. As shown in Figure 2c, comparison of the representative target plate before and after impact confirmed that local edge perforation occurred during the interaction with the impactor, accompanied by local plastic deformation near the impacted region.

The impactor was made of high-strength 35CrMnSiA steel. As confirmed by post-test examination, it underwent only elastic deformation, with no measurable permanent deformation or mass loss across all impacts, as shown in Figure 2b. This demonstrated that no cumulative damage or state evolution, such as work hardening or geometric blunting, occurred within the impactor itself.

The triple-impact configuration was designed to reproduce the sequential multiple-target impact process, in which the impactor successively interacted with three independent target plates and generated acceleration responses associated with local perforation and plastic deformation. The number of impacts was determined by the geometric constraints of the experimental setup, and three impacts were selected as a representative and practical case for developing the proposed predictive modeling framework.

3. Results

This section presents the experimental results obtained from the mechanical property tests and sequential multiple-target impact experiments. The quasi-static and dynamic mechanical properties of the nine target materials are first summarized, followed by the acceleration peaks and pulse durations extracted from the sequential multiple-target impact responses. These results provide the data foundation for the subsequent statistical analysis and quantitative model construction.

3.1. Mechanical Properties of Materials

The mechanical properties of the investigated materials are summarized in Table 2. The tested metallic materials showed significant variations in their quasi-static mechanical properties. Carbon steels (AISI 1020/1040/1060) demonstrated superior overall performance, particularly AISI 1060 steel, which showed an ultimate tensile strength of 690.0 MPa and a tensile yield strength of 306.3 MPa.

Table 2. Mechanical properties of the investigated materials.

Material	Elastic Modulus, GPa	Tensile Yield Strength, MPa	Ultimate Tensile Strength, MPa	Elongation, %	Compressive Yield Strength, MPa	Dynamic Compressive Yield Strength, MPa
AISI 1020 steel	235.0 ± 13.6	220.7 ± 0.9	386.7 ± 0.5	37.8 ± 1.2	585.9 ± 10.1	728.9
AISI 1040 steel	220.7 ± 7.1	301.7 ± 2.6	497.3 ± 3.1	31.5 ± 2.0	500.8 ± 15.8	803.1
AISI 1060 steel	217.7 ± 11.4	306.3 ± 3.9	690.0 ± 0.8	20.8 ± 0.2	1068.6 ± 11.5	1127.7
2A12 Al alloy	74.7 ± 1.7	349.7 ± 1.7	474.0 ± 2.2	20.7 ± 0.2	526.2 ± 17.6	462
7020 Al alloy	73.0 ± 1.6	518.7 ± 1.7	565.3 ± 0.9	11.5 ± 2.1	545.8 ± 18.5	583.1
7075 Al alloy	73.0 ± 1.4	565.7 ± 13.7	508.0 ± 2.2	10.5 ± 1.4	580.9 ± 11.0	621.5
AZ31B Mg alloy	46.0 ± 1.4	180.3 ± 4.5	246.0 ± 12.8	8.7 ± 1.0	115 ± 11.6	128.3
H62 brass	109.0 ± 2.8	284.7 ± 1.7	385.3 ± 5.7	42.0 ± 0.0	376.2 ± 17.1	315.5
S30153 stainless steel	202.7 ± 11.6	268 ± 2.2	581.3 ± 1.7	54.3 ± 0.6	758.8 ± 17.1	992.2

The corresponding mechanical property test curves are provided in the Supplementary Materials as Figure S1.

High-strength aluminum alloys (7075/7020) exhibited high strength (518.7 MPa and 565.7 MPa) but relatively low elongation. In contrast, AZ31B magnesium alloy and 2A12 aluminum alloy displayed lower elastic moduli (46.0 GPa and 74.7 GPa) and tensile yield strengths (180.3 MPa and 349.7 MPa), along with weaker compressive performance.

S30153 stainless steel exhibited the highest elongation (54.33%), indicating superior plastic deformation capacity, while H62 brass showed a balance between strength and

ductility with an elongation of 42%. These differences primarily originated from intrinsic variations in material composition and microstructure.

The reported values represent the effective properties of the as-received material batches, establishing a self-consistent dataset for the subsequent analysis of impact response.

3.2. Sequential Multiple-Target Impact Test Results

The peak values and durations corresponding to the three sequential impacts are shown in Table 3. Peak 1–Peak 3 represent the maximum acceleration amplitudes generated during the first, second, and third impact events, respectively, while Duration 1–Duration 3 refer to the corresponding pulse widths measured from pulse onset to return to the baseline.

Table 3. Acceleration parameters of sequential multiple-target impact events (peak in g, duration in μs, SD: standard deviation).

Material	No.	Peak 1	Duration 1	Peak 2	Duration 2	Peak 3	Duration 3
AISI 1020 steel	1	18,000	845	20,252	1025	19,612	1410
	2	17,570	760	19,521	735	20,495	865
	3	20,844	1020	19,738	900	20,281	785
	Average	18,805	875	19,837	887	20,129	1020
	SD	1452.7	108.2	306.5	118.8	376.1	277.7
AISI 1040 steel	1	22,979	570	28,954	620	24,886	585
	2	21,663	760	25,396	740	23,625	670
	3	23,054	836	22,514	688	25,661	752
	Average	22,565	722	25,621	683	24,724	669
	SD	638.8	111.9	2633.9	49.1	839	68.2
AISI 1060 steel	1	22,411	820	23,507	870	22,411	760
	2	20,413	960	20,911	740	20,911	810
	3	20,811	810	22,007	990	22,803	1010
	Average	21,212	863	22,142	867	22,042	860
	SD	863.5	68.5	1064.1	102.1	815.4	108
2A12 Al alloy	1	10,363	915	10,861	560	11,359	460
	2	12,705	525	8052	595	12,534	520
	3	12,948	880	12,450	965	12,948	650
	Average	12,005	773	10,454	707	12,280	543
	SD	1165.5	176.2	1818.4	183.2	673	79.3
7020 Al alloy	1	13,776	460	10,964	495	11,685	575
	2	16,231	665	14,411	465	14,555	360
	3	13,646	475	14,642	865	14,220	950
	Average	14,551	533	13,339	608	13,487	628
	SD	1189.1	93.3	1682	181.9	1281.3	243.8
7075 Al alloy	1	14,442	350	12,948	405	17,429	485
	2	15,934	750	16,548	825	16,548	700
	3	14,940	650	17,429	645	15,930	500
	Average	15,105	583	15,642	625	16,636	562
	SD	620.2	170	1938.4	172	615.1	98
AZ31B Mg alloy	1	6646	620	7144	665	5899	710
	2	6266	600	6640	545	9130	601
	3	4965	564	6957	474	5297	538
	Average	5959	595	6914	561	6775	616
	SD	719.8	23.2	208	78.8	1683	71.1

Table 3. *Cont.*

Material	No.	Peak 1	Duration 1	Peak 2	Duration 2	Peak 3	Duration 3
H62 brass	1	18,983	970	16,822	765	19,993	1070
	2	21,910	965	18,923	975	16,433	985
	3	19,501	722	17,666	687	17,121	961
	Average	20,131	886	17,804	809	17,849	1005
	SD	1275.4	115.7	863.2	121.6	1541.8	46.8
S30153 stainless steel	1	16,782	700	16,958	690	15,786	760
	2	19,919	740	18,516	780	18,249	660
	3	19,512	772	13,935	706	15,330	590
	Average	18,738	737	16,470	725	16,455	670
	SD	1392.8	29.5	1901.8	39.2	1282.1	69.8

The corresponding acceleration time-history curves obtained from the sequential multiple-target impact experiments are provided in the Supplementary Materials as Figure S2.

For peak acceleration, steels consistently demonstrated the highest peak values across all impacts (17,570–28,954 g), magnesium alloy (AZ31B) showed the lowest peak magnitudes (4965–9130 g), aluminum alloys exhibited intermediate peaks (8052–17,429 g), and brass and stainless steel displayed comparable peak values (13,935–21,910 g). The acceleration durations varied significantly by material: 570–1410 μs (AISI 1020, showing the widest pulses) for the steels, 350–965 μs (7075 alloy with the shortest pulses) for aluminum alloys, 474–710 μs (most consistent durations) for the magnesium alloy, and brass displayed the maximum duration (1070 μs). Progressive changes were observed during successive impacts, where AISI steels showed < 10% peak variation between impacts, aluminum alloys exhibited 15–25% fluctuations, and magnesium demonstrated the greatest variability up to a 35% difference.

4. Discussion

This section discusses the acceleration response characteristics, statistical significance, and quantitative prediction models obtained from the sequential multiple-target impact experiments. The effects of target material properties and target position in the impact sequence on acceleration peaks and pulse durations are first analyzed, followed by the construction and interpretation of regression-based prediction models. Finally, the influence patterns of material parameters and the corresponding material-selection strategy are discussed.

4.1. A Qualitative Comparison of Acceleration Signatures Between Single and Sequential Multiple-Target Impacts

A comparison of the experimental data reveals fundamental differences in the dynamic response between single-impact events (air cannon tests from Ref. [31]) and the sequential multiple-target impact scenario investigated in this study (Figure 3). Single impacts concentrate energy release through instantaneous collision, generating high-amplitude (approximately 40,000 g), short-duration (approximately 210 μs) pulses. In contrast, sequential multiple-target impacts distribute the impact process over successive interactions between the impactor and three independent target plates, exhibiting multiple and long-duration loading characteristics. Specifically, under broadly comparable impact energy conditions to the single impact reported in Ref. [31], the sequential multiple-target impacts showed a 3–4 fold increase in cumulative duration while the peak acceleration decreased by approximately 55%. This disparity may be attributed to different energy-transfer mechanisms. In sequential multiple-target impacts, the impactor successively interacts with indepen-

dent target plates, and stress-wave interaction, local perforation, plastic deformation, and residual vibration during successive impacts may contribute to a longer loading duration.

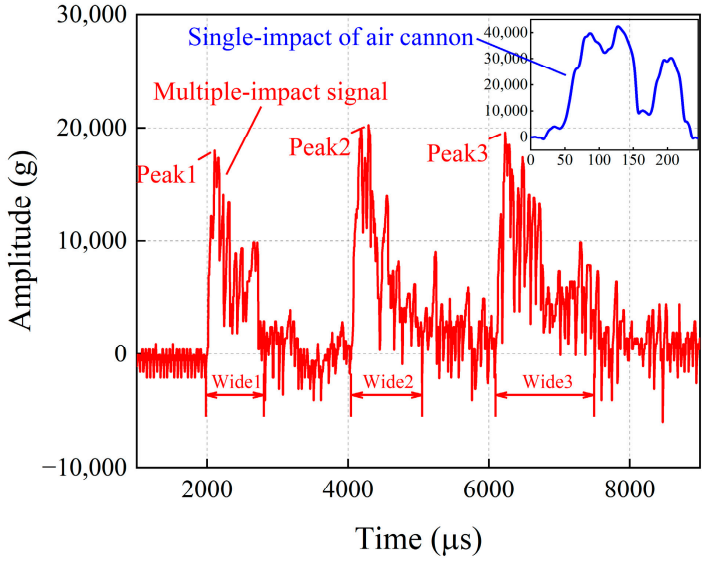

Figure 3. Comparison between sequential multiple-target impact and single-impact outcomes.

The sequential multiple-target impact test data indicated that stress-wave interaction and residual vibration may occur during successive impacts. As shown in Figure 3, compared with the first impact, the second and third impacts exhibited more evident local oscillations in the acceleration signals. This phenomenon may be related to stress-wave reflection and superposition during the successive interactions between the impactor and independent target plates. Therefore, the observed waveform variation can be regarded as a local dynamic response feature of sequential multiple-target impacts, rather than a dominant factor controlling the overall acceleration characteristics.

4.2. ANOVA of the Effects of Material Mechanical Properties on Acceleration Responses Under Sequential Multiple-Target Impact Conditions

This work employed two-factor ANOVA without replication to systematically investigate the effects of material type and target position in the impact sequence on acceleration responses. The statistical results (Tables 4 and 5) revealed that, for peak acceleration, material type had an extremely significant effect ($F = 79.43$, $p = 2.05 \times 10^{-11}$), whereas the target position in the impact sequence had no significant influence ($F = 0.12$, $p = 0.89$). For duration, the material type similarly had significant effects ($F = 12.30$, $p = 1.62 \times 10^{-5}$), whereas the effect of target position in the impact sequence remained non-significant ($F = 0.08$, $p = 0.92$). All analyses were performed using mean values from three independent experimental runs. (The calculations were performed using Microsoft Excel).

Consequently, during sequential multiple-target impact events, the mechanical properties of materials were the main factors governing acceleration response characteristics (both peak amplitude and duration). Their influence substantially surpassed that of target position in the impact sequence.

The non-significant effect of target position does not mean that the acceleration waveforms of the three impacts were completely identical. Instead, it indicates that the differences among the three target positions in peak acceleration and duration were relatively small compared with the differences caused by material type. Therefore, the local waveform variations observed in Figure 3 were not sufficient to produce a statistically significant independent effect of target position.

Table 4. ANOVA results of material mechanical properties' effects on peak acceleration in sequential multiple-target impact conditions.

Material	Peak 1	Peak 2	Peak 3			
AISI 1020 steel	18,805	19,837	20,129			
AISI 1040 steel	22,565	25,621	24,724			
AISI 1060 steel	21,212	22,142	22,042			
2A12 Al alloy	12,005	10,454	12,280			
7020 Al alloy	14,551	13,339	13,487			
7075 Al alloy	15,105	15,642	16,636			
AZ31B Mg alloy	5959	6914	6775			
H62 brass	20,131	17,804	17,849			
S30153 stainless steel	18,738	16,470	16,455			
ANOVA results						
Variation source	SS	df	MS	*F*	*p*-value	F crit
Target position	261,792.87	2	130,896.44	0.12	0.89	3.63
Material type	703,258,905	8	87,907,363	79.43	2.05×10^{-11}	2.59
Error	17,708,637	16	1106,789.8			
Total	721,229,336	26				

Table 5. ANOVA results of material mechanical properties' effects on duration in sequential multiple-target impact conditions.

Material	Duration 1	Duration 2	Duration 3			
AISI 1020 steel	875	887	1020			
AISI 1040 steel	722	683	669			
AISI 1060 steel	863	867	860			
2A12 Al alloy	773	707	543			
7020 Al alloy	533	608	628			
7075 Al alloy	583	625	562			
AZ31B Mg alloy	595	561	616			
H62 brass	886	809	1005			
S30153 stainless steel	737	725	670			
ANOVA results						
Variation source	SS	df	MS	*F*	*p*-value	F crit
Target position	719.73	2	359.86	0.08	0.92	3.63
Material type	446,538.50	8	55,817.31	12.3	1.62×10^{-5}	2.59
Error	72,602.27	16	4537.64			
Total	519,860.50	26				

4.3. Quantitative Model for the Effect of Material Mechanical Properties on Acceleration Characteristics Under Sequential Multiple-Target Impacts

This subsection presents the data preprocessing, regression model construction, model selection, and parameter influence analysis used to establish quantitative relationships between target material properties and acceleration characteristics.

4.3.1. Datasets and Preprocessing

This study encompasses a total of nine material sample groups. Each sample includes six material mechanical property parameters (elastic modulus, tensile yield strength, ultimate tensile strength, elongation, compressive yield strength, and dynamic compressive yield strength). The output Variables were the three sequential impact acceleration peaks and their corresponding pulse durations, namely Peak 1–Peak 3 and Duration 1–Duration 3.

Four distinct model fitting and data partitioning schemes were designed to ensure that the number of samples in each training set was greater than or equal to the number of input variables. These schemes include:

1. 9 samples for training with no dedicated test set;
2. 8 samples for training and 1 for testing;
3. 7 samples for training and 2 for testing;
4. 6 samples for training and 3 for testing.

Before regression modeling, only the input Variables were standardized to reduce the influence of different units and numerical scales among the material mechanical properties. The input Variables included elastic modulus, tensile yield strength, ultimate tensile strength, elongation, compressive yield strength, and dynamic compressive yield strength. Z-score normalization was used for this preprocessing step, where the mean value and standard deviation of each input Variable were calculated using Equations (1) and (2). The output Variables, including Peak 1–Peak 3 and Duration 1–Duration 3, were not standardized and were retained in their original units for model fitting and performance evaluation. This standardization refers to statistical data preprocessing rather than standardization according to an external testing standard. For each input Variable, z-score normalization was performed as follows:

$$Z = \frac{z - \overline{z}}{s_z} \tag{1}$$

where Z, z, $\overline{z}$, and, s_z are the standardized value, original value, mean, and standard deviation of the variable, respectively.

The standard deviation was calculated as:

$$s_z = \sqrt{\frac{1}{m}\left((z_1 - \overline{z})^2 + (z_2 - \overline{z})^2 + \cdots + (z_m - \overline{z})^2\right)} \tag{2}$$

where m represents the sample size, which in this context corresponds to the number of samples in the training set.

During the standardization process, only the mean ($\overline{z}$) and standard deviation (s_z) calculated from the training set were used for the transformation.

4.3.2. Regression Models

This study employs a suite of seven linear and regularized linear regression models, all of which are linear in nature. The selection of linear models is grounded in several key considerations. First, the limited sample size coupled with the approximately linear relationship between the material mechanical parameters and the Variables makes linear regression a suitable choice. Employing higher-order models, such as polynomial regression, would likely induce overfitting due to increased model complexity. While such complex models might perform well on the training data, they often suffer from poor generalizability in practical applications.

Second, regularized linear models provide an effective way to control model complexity. Ridge regression can reduce coefficient instability caused by multicollinearity by shrinking the regression coefficients, while Lasso regression can reduce model complexity by driving less important coefficients toward zero. Elastic Net combines the advantages of L1 and L2 regularization and can improve model stability when correlated input Variables are present.

Furthermore, linear models are characterized by lower computational complexity and offer superior interpretability. They allow for a clear elucidation of how individual material parameters influence the output Variables, which aligns well with the requirements for material design and performance optimization.

In summary, given the constraints of the sample size and the need to mitigate overfitting risks, linear models and their regularized variants are deemed more appropriate for this study. These models provide a balanced approach for obtaining preliminary empirical prediction models with reasonable fitting and generalization performance within the tested material range.

The specific models used in this study, along with their parameter configurations, are detailed in Table 6.

Table 6. Regression models and parameter configuration.

No.	Model Name	Parameter Configuration
1	Linear Regression	Default parameters
2	Ridge Regression	$\alpha = 0.1$
3	Ridge Regression	$\alpha = 1$
4	Ridge Regression	$\alpha = 10$
5	Lasso Regression	$\alpha = 0.01$
6	Lasso Regression	$\alpha = 0.1$
7	Elastic Net	$\alpha = 0.1$, $l_1 = 0.5$

The model performance is evaluated using the root mean square error (RMSE) and the mean absolute percentage error (MAPE).

RMSE quantifies the average magnitude of the absolute errors between predicted and measured values. Its unit matches that of the dependent variable, with a smaller RMSE indicating higher prediction accuracy of the model. The calculation formula is as follows:

$$RMSE = \sqrt{\frac{1}{m}\sum_{i=1}^{m}(y_i - \hat{y}_i)^2} \tag{3}$$

where y_i represents the true value of the dependent variable (either acceleration peak or pulse duration), $\hat{y}_i$ represents the predicted value of the predicted variable, and m is the number of samples.

MAPE measures the average relative deviation between predicted and measured values, expressed as a percentage. It provides a more intuitive assessment compared to RMSE and remains unaffected by the scale of the dependent variable. A smaller MAPE indicates better predictive performance. The calculation formula is as follows:

$$MAPE = \frac{1}{m}\sum_{i=1}^{m}\left|\frac{y_i - \hat{y}_i}{y_i}\right| \times 100\% \tag{4}$$

1. Linear regression model;

A linear regression model was constructed to analyze the relationship between the input Variables and output Variables. The six standardized mechanical property parameters, namely elastic modulus, tensile yield strength, ultimate tensile strength, elongation, compressive yield strength, and dynamic compressive yield strength, were used as input Variables. The acceleration peaks and pulse durations were used as output Variables. The regression equation is expressed as:

$$\hat{y} = b + \sum_{j=1}^{n}\omega_j x_j \tag{5}$$

where $\hat{y}$ represents the predicted value of the output variable (either acceleration peak or pulse duration), b is the bias term (intercept), and ω_j are the regression coefficients corresponding to each input variable.

The mean squared error (*MSE*) was employed as the loss function for the model, expressed as:

$$L_{MSE}(\omega) = \frac{1}{m}\sum_{i=1}^{m}(y_i - \hat{y}_i)^2 = \frac{1}{m}\sum_{i=1}^{m}\left(y_i - \left(b + \sum_{j=1}^{n}\omega_j x_{ij}\right)\right)^2 \quad (6)$$

where m denotes the number of samples in the training set, y_i represents the measured value of the output variable for the i-th sample, x_{ij} represents the j-th input variable of the i-th sample, and n stands for the number of input variables.

By taking the derivative of the loss function and setting it to zero, the analytical solution for the regression coefficients can be obtained:

$$\omega = \left(X^T X\right)^{-1} X^T y \quad (7)$$

where the matrix X represents the input variables (of dimension m × (n + 1), with its first column being a vector of ones corresponding to the intercept term), and y denotes the dependent variable vector (of dimension m × 1).

While linear regression models are suitable for simple scenarios where independent and output variables exhibit a linear relationship, they are prone to overfitting or unstable coefficient estimation when numerous input variables are involved or when multicollinearity exists. Regularized linear models address these issues by introducing a regularization term into the loss function to shrink the regression coefficients, thereby enhancing model stability and generalization capability. Therefore, three regularized linear models were considered in this study: Ridge regression, Lasso regression, and Elastic Net.

2. Ridge regression (L2 regularization);

An L2 regularization term is introduced into the loss function of the linear regression model described above. The weight of the regularization term is controlled by adjusting the regularization strength parameter α. A larger α imposes a stronger penalty on the regression coefficients, resulting in stronger coefficient shrinkage and improved model stability.

The loss function for Ridge regression is defined as:

$$L_{L2}(\omega) = \frac{1}{m}\sum_{i=1}^{m}(y_i - \hat{y}_i)^2 + \alpha\sum_{j=1}^{n}|\omega_j|^2 \quad (8)$$

where α denotes the regularization strength parameter (alpha). By penalizing the coefficients of the input variables, Ridge regression effectively reduces model complexity.

3. Lasso regression (L1 regularization);

An L1 regularization term, namely the sum of the absolute values of the regression coefficients, was incorporated into the linear regression loss function. The loss function of Lasso regression is formulated as:

$$L_{L1}(\omega) = \frac{1}{m}\sum_{i=1}^{m}(y_i - \hat{y}_i)^2 + \alpha\sum_{j=1}^{n}|\omega_j| \quad (9)$$

Through the application of L1 regularization to the model coefficients, when the regularization parameter α is sufficiently large, certain regression coefficients are driven to zero. Therefore, Lasso regression can reduce model complexity by eliminating less important input Variables, thereby mitigating overfitting.

4. Elastic Net;

Combining the advantages of both L1 and L2 regularization, Elastic Net adjusts the weighting between the two penalty terms through the parameter l_1. This approach retains the feature selection capability of Lasso while preserving the stability of Ridge regression. Its loss function is defined as:

$$L(\omega) = \frac{1}{m}\sum_{i=1}^{m}(y_i - \hat{y}_i)^2 + \alpha\left[l_1\sum_{j=1}^{n}|\omega_j| + (1-l_1)\sum_{j=1}^{n}|\omega_j|^2\right] \quad (10)$$

where $l_1 \in [0, 1]$. The model degenerates to Lasso when $l_1 = 1$ and to Ridge regression when $l_1 = 0$.

Considering the limited sample size, the model comparison was focused on linear and regularized linear regression models to avoid excessive model complexity and reduce overfitting risk.

4.3.3. Quantitative Model Construction

The regression models were constructed using six standardized mechanical-property parameters as input Variables, including elastic modulus x_1, tensile yield strength x_2, ultimate tensile strength x_3, elongation x_4, compressive yield strength x_5, and dynamic compressive yield strength x_6. The output Variables were the acceleration characteristics extracted from the sequential multiple-target impact experiments, including Peak 1–Peak 3 and Duration 1–Duration 3. Each output Variable was fitted separately using the regression models. The algorithms were implemented using Python 3.8.10.

The models were trained using their corresponding MSE-based loss functions. Specifically, linear regression minimized MSE, whereas Ridge regression, Lasso regression, and Elastic Net minimized MSE with the corresponding regularization terms. For model selection, Training MAPE (%) and Test MAPE (%) were used as the primary evaluation indicators when a test set was available. The model for each output Variable was selected by considering low MAPE values, small differences between Training MAPE and Test MAPE, and stable performance under different training–test partitioning schemes. RMSE was used as a complementary indicator to evaluate the absolute prediction error.

1. Training set with 9 groups and no test set;

All nine sample groups were utilized as the training set without a dedicated test set to evaluate the models' fitting performance on the available data. A comparison of the fitting results across the models is presented in Table 7. The findings indicate that the linear regression and Lasso regression models generally delivered the best overall performance. For Peak 1–Peak 3 and Duration 1–Duration 2, these models yielded lower MAPE and maximum relative error values compared to other models, with the exception of the Ridge regression model with α = 0.1. As the regularization parameter α increases in Ridge regression, there is a corresponding rise in RMSE, MAPE, and maximum relative error. The Elastic Net model performed intermediately between linear/Lasso regression and Ridge regression but is generally outperformed by the former two. Furthermore, the results suggest that Duration 2 is relatively easier to fit, with notably smaller errors compared to other Variables, whereas Duration 3 presents the highest fitting difficulty, consistently showing maximum relative errors exceeding 24%.

Based on the lowest RMSE and MAPE values, the selected models for each acceleration peak and duration characteristic under this partitioning scheme are summarized in Table 8. For the acceleration peaks, Peak 1 demonstrates the best fitting performance, with its RMSE, MAPE, and maximum relative error all lower than those of Peak 2 and Peak 3. In contrast, both Peak 2 and Peak 3 exhibit maximum relative errors exceeding 15%, indicating relatively poor fitting quality. Regarding the durations, Duration 2 achieves the

best fit, followed by Duration 1. Although Duration 3 shows a MAPE of 14.03%, its maximum relative error reaches 24.60%, representing the weakest fitting performance among all characteristics.

Table 7. Comparison of model fitting results using 9 training groups without a test group.

Variable	Model	RMSE	MAPE (%)	Max Relative Error (%)
Peak 1	Linear Regression	1254.62	7.49	13.43
	Ridge Regression ($\alpha = 0.1$)	1429.16	7.82	12.77
	Ridge Regression ($\alpha = 1$)	2128.32	11.93	31.78
	Ridge Regression ($\alpha = 10$)	2870.32	18.38	79.54
	Lasso Regression ($\alpha = 0.01$)	1254.62	7.49	13.43
	Lasso Regression ($\alpha = 0.1$)	1254.63	7.49	13.43
	Elastic Net ($\alpha = 0.1$, $l_1 = 0.5$)	1879.33	10.35	21.14
Peak 2	Linear Regression	1652.83	9.7	19.52
	Ridge Regression ($\alpha = 0.1$)	1792.59	10.24	15.67
	Ridge Regression ($\alpha = 1$)	2507	14.38	24.24
	Ridge Regression ($\alpha = 10$)	3472.75	21.12	56.94
	Lasso Regression ($\alpha = 0.01$)	1652.83	9.7	19.52
	Lasso Regression ($\alpha = 0.1$)	1652.83	9.7	19.51
	Elastic Net ($\alpha = 0.1$, $l_1 = 0.5$)	2210.56	12.76	19.81
Peak 3	Linear Regression	1503.38	7.55	20.72
	Ridge Regression ($\alpha = 0.1$)	1641.69	9.08	17.51
	Ridge Regression ($\alpha = 1$)	2324.92	13.31	30.06
	Ridge Regression ($\alpha = 10$)	3214.31	20.3	64.71
	Lasso Regression ($\alpha = 0.01$)	1503.38	7.55	20.72
	Lasso Regression ($\alpha = 0.1$)	1503.38	7.55	20.72
	Elastic Net ($\alpha = 0.1$, $l_1 = 0.5$)	2046.41	11.68	21.76
Duration 1	Linear Regression	27.15	3.27	9.95
	Ridge Regression ($\alpha = 0.1$)	34.82	4.47	9.31
	Ridge Regression ($\alpha = 1$)	66.13	8	13.86
	Ridge Regression ($\alpha = 10$)	87.79	11.72	21.15
	Lasso Regression ($\alpha = 0.01$)	27.15	3.28	9.94
	Lasso Regression ($\alpha = 0.1$)	27.17	3.33	9.85
	Elastic Net ($\alpha = 0.1$, $l_1 = 0.5$)	55.06	6.33	12.08
Duration 2	Linear Regression	0.77	0.09	0.23
	Ridge Regression ($\alpha = 0.1$)	18.43	2.18	4.47
	Ridge Regression ($\alpha = 1$)	53.93	6.5	11.52
	Ridge Regression ($\alpha = 10$)	73.64	9.43	14.38
	Lasso Regression ($\alpha = 0.01$)	0.78	0.09	0.22
	Lasso Regression ($\alpha = 0.1$)	1.32	0.16	0.29
	Elastic Net ($\alpha = 0.1$, $l_1 = 0.5$)	42.14	5	9.56
Duration 3	Linear Regression	67.93	7.7	30.37
	Ridge Regression ($\alpha = 0.1$)	75.6	9.04	27.93
	Ridge Regression ($\alpha = 1$)	113.82	14.03	24.6
	Ridge Regression ($\alpha = 10$)	138.72	16.09	27.08
	Lasso Regression ($\alpha = 0.01$)	67.93	7.7	30.36
	Lasso Regression ($\alpha = 0.1$)	67.94	7.67	30.32
	Elastic Net ($\alpha = 0.1$, $l_1 = 0.5$)	99.56	12.45	25.36

Table 8. Selected models for each acceleration peak and duration using 9 training groups without a test group.

Feature	Optimal Model	RMSE	MAPE (%)	Maximum Relative Error (%)
Peak 1	Linear Regression	1254.62	7.49	13.43
Peak 2	Ridge Regression (α = 0.1)	1792.59	10.24	15.67
Peak 3	Ridge Regression (α = 0.1)	1641.69	9.08	17.51
Duration 1	Linear Regression	27.15	3.27	9.95
Duration 2	Linear Regression	0.77	0.09	0.23
Duration 3	Ridge Regression (α = 1)	113.82	14.03	24.60

The fitted formula is expressed as follows:

$$\begin{cases} y_{p1} = 16563.4 + 9052.4x_1 + 2472.0x_2 + 5055.7x_3 + 1139.7x_4 + 643.3x_5 - 9173.3x_6 \\ y_{p2} = 16469.2 + 8782.8x_1 + 2382.0x_2 + 2752.0x_3 - 416.9x_4 - 1083.1x_5 - 4454.1x_6 \\ y_{p3} = 16708.6 + 8153.1x_1 + 2654.6x_2 + 1945.4x_3 - 213.5x_4 + 67.2x_5 - 4603.1x_6 \\ y_{w1} = 729.7 + 176.5x_1 - 9.8x_2 + 20.2x_3 + 35.5x_4 + 238.8x_5 - 351.9x_6 \\ y_{w2} = 719.1 + 159.5x_1 + 22.4x_2 - 29.1x_3 + 20.6x_4 + 236.6x_5 - 276.0x_6 \\ y_{w3} = 730.3 + 88.5x_1 - 9.6x_2 - 54.7x_3 + 39.9x_4 + 86.8x_5 - 83.2x_6 \end{cases} \quad (11)$$

2. Training set with 8 groups and test set with 1 group;

One group of samples was used as the test set to evaluate the model's generalization capability on unseen data. The fitting results for all models are presented in Table 9. Linear regression and Lasso regression demonstrated strong overall fitting performance on the training set but exhibited a risk of overfitting for Peak 1 and Peak 2, with test set MAPE exceeding 21%. For Peak 3, Duration 1–Duration 3, these models simultaneously achieved balanced performance in both fitting and generalization, with MAPE values below 15% for both training and test sets.

Table 9. Comparison of model fitting and generalization results using 8 training groups and 1 test group.

Variable	Model	Training RMSE	Test RMSE	Training MAPE (%)	Test MAPE (%)
Peak 1	Linear Regression	1004.23	3622.91	5.79	24.9
	Ridge Regression (α = 0.1)	1336.27	2371.63	6.69	16.3
	Ridge Regression (α = 1)	2232.68	889.79	13.08	6.11
	Ridge Regression (α = 10)	3039.75	896.33	20.6	6.16
	Lasso Regression (α = 0.01)	1004.23	3622.67	5.79	24.9
	Lasso Regression (α = 0.1)	1004.23	3620.52	5.78	24.88
	Elastic Net (α = 0.1, l_1 = 0.5)	1905.37	1345.24	10.76	9.24
Peak 2	Linear Regression	1628.44	2214.78	8.08	21.19
	Ridge Regression (α = 0.1)	1810.32	2067.69	10.36	19.78
	Ridge Regression (α = 1)	2611.04	2821.06	14.54	26.99
	Ridge Regression (α = 10)	3490.21	4695.72	20.18	44.92
	Lasso Regression (α = 0.01)	1628.44	2214.77	8.08	21.19
	Lasso Regression (α = 0.1)	1628.44	2214.68	8.08	21.19
	Elastic Net (α = 0.1, l_1 = 0.5)	2251.78	2285.57	12.84	21.86
Peak 3	Linear Regression	1583.57	638.15	7.75	5.2
	Ridge Regression (α = 0.1)	1744.15	494.26	10.06	4.02
	Ridge Regression (α = 1)	2484.46	1207.37	14.52	9.83
	Ridge Regression (α = 10)	3355.71	3005.72	21.11	24.48
	Lasso Regression (α = 0.01)	1583.57	638.09	7.75	5.2
	Lasso Regression (α = 0.1)	1583.57	637.55	7.75	5.19
	Elastic Net (α = 0.1, l_1 = 0.5)	2143.88	695.52	12.68	5.66

Table 9. *Cont.*

Variable	Model	Training RMSE	Test RMSE	Training MAPE (%)	Test MAPE (%)
Duration 1	Linear Regression	21.41	122.9	2.33	14.05
	Ridge Regression ($\alpha = 0.1$)	35.89	30.78	4.59	3.52
	Ridge Regression ($\alpha = 1$)	70.96	65.03	8.55	7.43
	Ridge Regression ($\alpha = 10$)	91.31	99.63	11.87	11.39
	Lasso Regression ($\alpha = 0.01$)	21.42	122.16	2.33	13.96
	Lasso Regression ($\alpha = 0.1$)	21.47	115.64	2.41	13.22
	Elastic Net ($\alpha = 0.1$, $l_1 = 0.5$)	58.75	40.77	7.11	4.66
Duration 2	Linear Regression	0.8	0.5	0.1	0.07
	Ridge Regression ($\alpha = 0.1$)	20.74	13.12	2.47	1.86
	Ridge Regression ($\alpha = 1$)	57.89	32.78	6.84	4.64
	Ridge Regression ($\alpha = 10$)	77.99	25.26	10.14	3.57
	Lasso Regression ($\alpha = 0.01$)	0.81	0.53	0.1	0.07
	Lasso Regression ($\alpha = 0.1$)	1.32	0.79	0.16	0.11
	Elastic Net ($\alpha = 0.1$, $l_1 = 0.5$)	43.96	26.36	5.1	3.73
Duration 3	Linear Regression	72.05	3.7	8.68	0.36
	Ridge Regression ($\alpha = 0.1$)	81.87	103.79	9.43	10.18
	Ridge Regression ($\alpha = 1$)	114.93	223.2	12.78	21.88
	Ridge Regression ($\alpha = 10$)	130.41	266.93	14.19	26.17
	Lasso Regression ($\alpha = 0.01$)	72.05	2.97	8.67	0.29
	Lasso Regression ($\alpha = 0.1$)	72.06	3.55	8.6	0.35
	Elastic Net ($\alpha = 0.1$, $l_1 = 0.5$)	102.89	189.31	11.54	18.56

Similarly, the generalization ability of Ridge regression varied with the regularization parameter α. Generally, MAPE increased as α grew, but for the Variable Peak 1, a smaller α resulted in higher test set MAPE, whereas a larger α reduced it. Elastic Net showed intermediate performance between linear regression, Lasso regression, and Ridge regression, without a distinct advantage, yet performed well in both fitting and generalization for Peak 1.

Additionally, Duration 2 showed relatively low fitting and generalization difficulty, with linear regression and Lasso regression achieving excellent results, whereas Peak 2 demonstrated the poorest generalization performance, with MAPE consistently above 19%.

Based on the lowest RMSE and MAPE values, the selected models for each acceleration peak and duration characteristic under this partitioning scheme are summarized in Table 10. For the acceleration peaks, the training set results for Peaks 1–3 all exhibit MAPE values below 11%, indicating good fitting performance. However, based on the test set MAPE, Peak 3 demonstrates the best generalization capability, with both RMSE and MAPE lower than those of Peak 1 and Peak 2. In contrast, Peak 2 shows a relatively poor generalization performance, with a MAPE reaching 19.78%. As for the durations, both training and test set results achieve MAPE values below 10%, reflecting favorable fitting and generalization outcomes. Among these, Duration 2 performs the best.

Table 10. Selected models for each acceleration peak and duration using 8 training groups and 1 test group.

Variable	Test Set Selection (Material)	Selected Model	Training RMSE	Training MAPE (%)	Test RMSE	Test MAPE (%)
Peak 1	7020 Al alloy	Elastic Net ($\alpha = 0.1$, $l_1 = 0.5$)	1905.37	10.76	1345.2	9.24
Peak 2	2A12 Al alloy	Ridge Regression ($\alpha = 0.1$)	1810.32	10.36	2067.7	19.78
Peak 3	2A12 Al alloy	Linear Regression	1583.57	7.75	638.2	5.2
Duration 1	AISI 1020 steel	Ridge Regression ($\alpha = 0.1$)	35.89	4.59	30.8	3.52

Table 10. *Cont.*

Variable	Test Set Selection (Material)	Selected Model	Training RMSE	Training MAPE (%)	Test RMSE	Test MAPE (%)
Duration 2	2A12 Al alloy	Linear Regression	0.8	0.1	0.5	0.07
Duration 3	AISI 1020 steel	Lasso Regression (α = 0.01)	72.05	8.67	2.97	0.29

The fitted equations are given as follows:

$$\begin{cases} y_{p1} = 16815.0 + 4410.3x_1 + 1791.3x_2 + 1824.4x_3 + 1539.2x_4 - 166.4x_5 - 2105.2x_6 \\ y_{p2} = 17221.1 + 8527.1x_1 + 2334.6x_2 + 3067.9x_3 - 366.9x_4 - 751.0x_5 - 4977.2x_6 \\ y_{p3} = 17262.1 + 10495.6x_1 + 3064.6x_2 + 3907.6x_3 - 505.5x_4 + 596.3x_5 - 8645.7x_6 \\ y_{w1} = 711.5 + 114.5x_1 - 14.6x_2 - 26.0x_3 + 40.1x_4 + 212.3x_5 - 243.9x_6 \\ y_{w2} = 720.6 + 160.9x_1 + 23.8x_2 - 30.9x_3 + 21.7x_4 + 250.5x_5 - 285.9x_6 \\ y_{w3} = 694.1 + 310.3x_1 + 56.8x_2 - 23.9x_3 + 27.9x_4 + 337.3x_5 - 553.5x_6 \end{cases} \quad (12)$$

3. Training set with 7 groups and test set with 2 groups;

Two sample groups were used as the test set to assess the models' generalization performance on unseen data. The fitting results for all models are presented in Table 11. Linear regression and Lasso regression again exhibited a risk of overfitting: except for Duration 2, their test set RMSE and MAPE values were higher than those of the other models, with the test set RMSE reaching up to 35,106.01 and MAPE reaching 185.64%. Ridge regression and Elastic Net effectively mitigated overfitting and demonstrated superior performance, with most Variables being best fitted by these two models. Notably, as the regularization parameter α increased in Ridge regression, the training set MAPE also increased. At α values of 0.1 and 1, the training set MAPE results remained favorable. Consistently, Duration 2 demonstrated strong fitting and generalization performance, whereas Peak 2 exhibited relatively weak generalization ability.

Table 11. Comparison of model fitting and generalization results using 7 training groups and 2 test groups.

Variable	Model	Training RMSE	Test RMSE	Training MAPE (%)	Test MAPE (%)
Peak 1	Linear Regression	0	30,978.79	0	163.67
	Ridge Regression (α = 0.1)	1429.88	3229.23	7.07	11.78
	Ridge Regression (α = 1)	2156.68	3192.21	12.63	10.69
	Ridge Regression (α = 10)	2908.23	3654.52	20.83	13.01
	Lasso Regression (α = 0.01)	56.56	29,433.86	0.33	155.75
	Lasso Regression (α = 0.1)	12.05	30,648.54	0.07	161.98
	Elastic Net (α = 0.1, l_1 = 0.5)	1828.1	3229.11	9.78	10.92
Peak 2	Linear Regression	0	35,106.01	0	185.64
	Ridge Regression (α = 0.1)	1566.13	4728.94	8.37	18.16
	Ridge Regression (α = 1)	2252.18	5194.7	14.3	18.43
	Ridge Regression (α = 10)	2949.79	6109.18	21.99	22.14
	Lasso Regression (α = 0.01)	51.11	33,713	0.31	178.64
	Lasso Regression (α = 0.1)	12.28	34,770	0.08	183.95
	Elastic Net (α = 0.1, l_1 = 0.5)	1918.2	4962.43	10.93	17.79
Peak 3	Linear Regression	0	7839.83	0	34.69
	Ridge Regression (α = 0.1)	1472.35	3100.24	8.59	13.38
	Ridge Regression (α = 1)	2597.01	1270.39	15.24	8.32
	Ridge Regression (α = 10)	3542.49	2125.06	23.08	14.69
	Lasso Regression (α = 0.01)	10.8	7804.66	0.06	34.55
	Lasso Regression (α = 0.1)	12.39	7798.18	0.07	34.52
	Elastic Net (α = 0.1, l_1 = 0.5)	2155.17	1471.19	12.74	7.42

Table 11. *Cont.*

Variable	Model	Training RMSE	Test RMSE	Training MAPE (%)	Test MAPE (%)
Duration 1	Linear Regression	0	166.9	0	18.79
	Ridge Regression (α = 0.1)	34.2	54.46	4.44	6.57
	Ridge Regression (α = 1)	78.51	32.84	10.23	4.29
	Ridge Regression (α = 10)	97.4	69.62	13.2	10.84
	Lasso Regression (α = 0.01)	0.14	165.98	0.02	18.63
	Lasso Regression (α = 0.1)	1.3	159.15	0.16	17.51
	Elastic Net (α = 0.1, l_1 = 0.5)	61.8	1.82	7.99	0.27
Duration 2	Linear Regression	0	12.6	0	1.93
	Ridge Regression (α = 0.1)	24.53	57.64	3.12	7.94
	Ridge Regression (α = 1)	58.95	83.46	7.39	11.66
	Ridge Regression (α = 10)	76.13	86.49	9.65	13.37
	Lasso Regression (α = 0.01)	0.47	1.81	0.05	0.28
	Lasso Regression (α = 0.1)	1.78	28.24	0.21	4.04
	Elastic Net (α = 0.1, l_1 = 0.5)	45.59	76.36	5.73	10.45
Duration 3	Linear Regression	0	682.73	0	84.07
	Ridge Regression (α = 0.1)	76.16	114.1	8.77	13.85
	Ridge Regression (α = 1)	122.93	154.36	13.6	14.17
	Ridge Regression (α = 10)	139.61	189.04	16.14	14.03
	Lasso Regression (α = 0.01)	0.27	680.43	0.03	83.8
	Lasso Regression (α = 0.1)	2.54	660.8	0.3	81.5
	Elastic Net (α = 0.1, l_1 = 0.5)	106.43	120.35	11.9	13.58

Based on the lowest RMSE and MAPE values, the selected models for each acceleration peak and duration characteristic under this partitioning scheme are summarized in Table 12. For the acceleration peaks, the training set results for Peaks 1–3 all achieved MAPE values below 9%. However, based on the test set results, Peak 1 demonstrated the best generalization performance, with both RMSE and MAPE lower than those of Peak 2 and Peak 3. In contrast, Peak 2 exhibited relatively poor generalization, with a test MAPE as high as 18.16%. Regarding the durations, both training and test set results showed MAPE values below 14%, indicating favorable fitting performance. Among these, Duration 1 achieved the best fitting and generalization results, followed by Duration 2.

Table 12. Selected models for each acceleration peak and duration using 7 training groups and 2 test groups.

Variable	Test Set (Materials)	Selected Model	Training RMSE	Training MAPE (%)	Test RMSE	Test MAPE (%)
Peak 1	AISI 1040 steel, 7020 Al alloy	Ridge Regression (α = 0.1)	1429.88	7.07	3229.23	11.78
Peak 2	AISI 1040 steel, 7020 Al alloy	Ridge Regression (α = 0.1)	1566.13	8.37	4728.94	18.16
Peak 3	2A12 Al alloy, 7075 Al alloy	Ridge Regression (α = 0.1)	1472.35	8.59	3100.24	13.38
Duration 1	AISI 1040 steel, 7075 Al alloy	Ridge Regression (α = 0.1)	34.2	4.44	54.46	6.57
Duration 2	AISI 1040 steel, 7020 Al alloy	Lasso Regression (α = 0.01)	0.47	0.05	1.81	0.28
Duration 3	AISI 1020 steel, 7020 Al alloy	Ridge Regression (α = 0.1)	76.16	8.77	114.1	13.85

The corresponding fitting equations are as follows:

$$\begin{cases} y_{p1} = 15993.6 + 4680.8x_1 + 2062.2x_2 + 1520.5x_3 + 2009.3x_4 + 3313.7x_5 - 5773.6x_6 \\ y_{p2} = 15609.0 + 6021.0x_1 + 2233.2x_2 + 534.6x_3 + 293.0x_4 + 2948.6x_5 - 4940.9x_6 \\ y_{p3} = 17351.6 + 8733.6x_1 + 1055.3x_2 + 4538.0x_3 - 254.8x_4 - 783.4x_5 - 6587.3x_6 \\ y_{w1} = 751.7 + 78.8x_1 - 23.9x_2 - 35.5x_3 + 50.8x_4 + 257.5x_5 - 250.9x_6 \\ y_{w2} = 740.1 + 159.1x_1 + 21.1x_2 - 32.1x_3 + 21.8x_4 + 266.3x_5 - 305.8x_6 \\ y_{w3} = 703.6 + 203.3x_1 + 23.9x_2 - 143.6x_3 + 44.6x_4 + 320.6x_5 - 336.8x_6 \end{cases} \quad (13)$$

4. Training set with 6 groups and test set with 3 groups;

With three sample groups used as the test set, the model's generalization ability on unseen data was evaluated. The fitting results of all models are presented in Table 13. Linear regression and Lasso regression again exhibited severe overfitting, with excessively high test set RMSE and MAPE values, except for Duration 2. The maximum test set RMSE reached 10,056.41, and MAPE reached 102.44%. Ridge regression and Elastic Net models performed well overall, effectively mitigating overfitting through regularization. Among these, for the fitting results of Peak 1–Peak 3 Variables in Ridge regression, both RMSE and MAPE increased as the regularization parameter α increased. Similarly, the Duration 2 Variable was the easiest to fit and generalize, while Duration 3 was more challenging to generalize, with the selected model achieving a test set MAPE of 15.92%.

Table 13. Comparison of model fitting and generalization results using 6 training groups and 3 test groups.

Variable	Model	Training RMSE	Test RMSE	Training MAPE (%)	Test MAPE (%)
Peak 1	Linear Regression	0	10,056.41	0	102.44
	Ridge Regression ($\alpha = 0.1$)	1474.83	2747.45	7.67	8.36
	Ridge Regression ($\alpha = 1$)	2138.99	4846.14	10.95	47.77
	Ridge Regression ($\alpha = 10$)	2387.79	6038.87	11.56	62.03
	Lasso Regression ($\alpha = 0.01$)	14	8135.09	0.07	86.4
	Lasso Regression ($\alpha = 0.1$)	2.67	8197.81	0.01	87.08
	Elastic Net ($\alpha = 0.1$, $l_1 = 0.5$)	1912.11	3662.26	9.92	33.43
Peak 2	Linear Regression	0	7731.38	0	26.51
	Ridge Regression ($\alpha = 0.1$)	1291.48	3475.46	7.73	14.07
	Ridge Regression ($\alpha = 1$)	2447.19	4859.27	15.47	18
	Ridge Regression ($\alpha = 10$)	2979.06	5859.61	22.03	22.32
	Lasso Regression ($\alpha = 0.01$)	6.88	7674.1	0.05	25.73
	Lasso Regression ($\alpha = 0.1$)	1.01	7642.13	0.01	25.56
	Elastic Net ($\alpha = 0.1$, $l_1 = 0.5$)	1982.53	3637.44	12.04	11.96
Peak 3	Linear Regression	0	4911.2	0	17.2
	Ridge Regression ($\alpha = 0.1$)	1136.37	3037.46	6.53	14.14
	Ridge Regression ($\alpha = 1$)	2181.87	4928.32	13.48	22
	Ridge Regression ($\alpha = 10$)	2759.93	5417.43	20.64	23.17
	Lasso Regression ($\alpha = 0.01$)	5.62	4798.47	0.03	20.68
	Lasso Regression ($\alpha = 0.1$)	0.67	4771.18	0	20.59
	Elastic Net ($\alpha = 0.1$, $l_1 = 0.5$)	1753.82	4012.75	10.27	16.94
Duration 1	Linear Regression	0	150.99	0	19.17
	Ridge Regression ($\alpha = 0.1$)	38.85	85.61	5.23	11.09
	Ridge Regression ($\alpha = 1$)	85.59	35.62	11.66	4.01
	Ridge Regression ($\alpha = 10$)	103.98	73.28	14.19	9.92
	Lasso Regression ($\alpha = 0.01$)	0.09	190.93	0.01	26.75
	Lasso Regression ($\alpha = 0.1$)	1.03	146.91	0.12	18.05
	Elastic Net ($\alpha = 0.1$, $l_1 = 0.5$)	65.31	42.97	8.83	4.96
Duration 2	Linear Regression	0	2.3	0	0.27
	Ridge Regression ($\alpha = 0.1$)	22.59	118.33	2.67	15.4
	Ridge Regression ($\alpha = 1$)	42.37	146.8	5.21	18.68
	Ridge Regression ($\alpha = 10$)	65.67	119.89	8.01	16.61
	Lasso Regression ($\alpha = 0.01$)	0.18	17.44	0.02	1.93
	Lasso Regression ($\alpha = 0.1$)	1.91	21.98	0.22	3.15
	Elastic Net ($\alpha = 0.1$, $l_1 = 0.5$)	32.18	151.06	3.7	19.64

Table 13. *Cont.*

Variable	Model	Training RMSE	Test RMSE	Training MAPE (%)	Test MAPE (%)
Duration 3	Linear Regression	0	401.21	0	53.52
	Ridge Regression (α = 0.1)	70.93	143.58	8.82	15.92
	Ridge Regression (α = 1)	125.33	144.87	14.92	18.84
	Ridge Regression (α = 10)	145.43	157.46	17.91	15.48
	Lasso Regression (α = 0.01)	0.2	377.13	0.02	51.72
	Lasso Regression (α = 0.1)	1.85	390.52	0.23	49.95
	Elastic Net (α = 0.1, l_1 = 0.5)	104.06	114.56	12.81	16.1

Based on the lowest RMSE and MAPE values, the selected models for each acceleration peak and duration characteristic under this partitioning scheme are summarized in Table 14. For the acceleration peaks, both the training and test set results for Peaks 1–3 all achieved MAPE values below 15%, with Peak 1 demonstrating relatively better generalization performance. Regarding the durations, the training set results exhibited MAPE values below 9%, indicating favorable fitting performance. Among these, Duration 2 achieved the best fitting results, whereas Duration 3 showed a test set MAPE exceeding 15%, reflecting relatively poor generalization capability.

Table 14. Selected models for each acceleration peak and duration using 6 training groups and 3 test groups.

Variable	Test Set (Materials)	Selected Model	Training RMSE	Training MAPE (%)	Test RMSE	Test MAPE (%)
Peak 1	AISI 1040 steel, 7020 Al alloy, AZ31B Mg alloy	Ridge Regression (α = 0.1)	1474.83	7.67	2747.45	8.36
Peak 2	AISI 1020 steel, AISI 1040 steel, 7020 Al alloy	Ridge Regression (α = 0.1)	1291.48	7.73	3475.46	14.07
Peak 3	AISI 1020 steel, AISI 1040 steel, 7020 Al alloy	Ridge Regression (α = 0.1)	1136.37	6.53	3037.46	14.14
Duration 1	AISI 1020 steel, AISI 1040 steel, 7075 Al alloy	Elastic Net (α = 0.1, l_1 = 0.5)	65.31	8.83	42.97	4.96
Duration 2	AISI 1020 steel, 7075 Al alloy, AZ31B Mg alloy	Linear Regression	0	0	2.3	0.27
Duration 3	AISI 1020 steel, 7020 Al alloy, AZ31B Mg alloy	Ridge Regression (α = 0.1)	70.93	8.82	143.58	15.92

The fitted equations are expressed as follows:

$$\begin{cases} y_{p1} = 17666.0 + 4589.1x_1 + 2025.2x_2 + 1303.9x_3 + 1901.8x_4 + 2958.1x_5 - 5543.8x_6 \\ y_{p2} = 14904.3 + 7889.0x_1 + 3178.3x_2 - 1319.5x_3 - 167.2x_4 + 3078.7x_5 - 5545.5x_6 \\ y_{p3} = 15339.5 + 6222.1x_1 + 2980.0x_2 - 248.9x_3 + 172.8x_4 + 3493.0x_5 - 5672.6x_6 \\ y_{w1} = 731.2 + 30.4x_1 - 40.3x_2 + 7.3x_3 + 49.0x_4 + 147.8x_5 - 139.4x_6 \\ y_{w2} = 733.2 + 140.5x_1 + 16.1x_2 - 23.5x_3 + 20.0x_4 + 219.5x_5 - 264.1x_6 \\ y_{w3} = 718.2 + 216.3x_1 - 37.5x_2 - 172.4x_3 + 42.7x_4 + 331.9x_5 - 305.8x_6 \end{cases} \quad (14)$$

5. Final optimized models.

The final optimized models are determined by systematically comparing performance metrics (RMSE and MAPE) across various training–test partitioning schemes, combined with an assessment of model stability on the training set and generalization capability on the test set. The optimal results are as summarized in Table 15.

Table 15. Final optimized models for acceleration peaks and durations.

Variable	Final Optimized Model	Key Rationale
Peak 1	Ridge Regression (α = 0.1)	Showed stable overall performance across different data partitions, with relatively low test set MAPE values (8.36–16.30%) and better generalization performance than linear regression and Lasso regression.
Peak 2	Ridge Regression (α = 0.1)	Balances training and test errors well and reduces the risk of overfitting compared with other regression models.
Peak 3	Ridge Regression (α = 0.1)	Achieved the lowest test set MAPE of 4.02% under the partitioning scheme with eight training groups and one test group, while maintaining stable performance across different data partitions.
Duration 1	Ridge Regression (α = 0.1)	Showed low test set MAPE values (3.52–11.09%) and a relatively small gap between training and test errors across different data partitions.
Duration 2	Linear Regression	Exhibited extremely low training and test errors, with MAPE values generally below 2% in almost all data partitions. The model was simple and showed no obvious overfitting.
Duration 3	Ridge Regression (α = 0.1)	Showed the best overall balance between fitting accuracy and generalization stability among the tested models, with relatively low test set MAPE values in most data partitions compared with Lasso regression and Elastic Net.

The fitted models for each acceleration peak and duration were established as follows:

$$\begin{cases} y_{p1} = 17666.0 + 4589.1x_1 + 2025.2x_2 + 1303.9x_3 + 1901.8x_4 + 2958.1x_5 - 5543.8x_6 \\ y_{p2} = 14904.3 + 7889.0x_1 + 3178.3x_2 - 1319.5x_3 - 167.2x_4 + 3078.7x_5 - 5545.5x_6 \\ y_{p3} = 17262.1 + 8087.9x_1 + 2757.5x_2 + 2055.7x_3 - 202.9x_4 + 151.9x_5 - 4763.7x_6 \\ y_{w1} = 711.5 + 114.5x_1 - 14.6x_2 - 26.0x_3 + 40.1x_4 + 212.3x_5 - 243.9x_6 \\ y_{w2} = 720.6 + 160.9x_1 + 23.8x_2 - 30.9x_3 + 21.7x_4 + 250.5x_5 - 285.9x_6 \\ y_{w3} = 694.1 + 187.4x_1 + 17.4x_2 - 5.7x_3 + 37.4x_4 + 218.2x_5 - 350.3x_6 \end{cases} \quad (15)$$

The final optimized models provide a preliminary quantitative description of the relationship between material mechanical properties and acceleration characteristics within the investigated material range. Since the models were developed using nine metallic materials, their applicability is currently limited to materials with mechanical-property ranges comparable to those tested in this study. Regularized regression methods, particularly Ridge regression, were introduced to improve model stability and reduce overfitting. Nevertheless, the limited dataset may still affect the robustness and generalization capability of the models. Therefore, the predicted values and regression coefficients should be interpreted as data-driven correlations within the present dataset. Further validation with a larger material database is needed to improve the reliability and broader applicability of the proposed models.

4.3.4. Influence Analysis Based on Quantitative Models

Based on the quantitative models given in Equation (15), the effects of material mechanical properties on the two categories of acceleration characteristics, namely acceleration peaks and pulse durations, were further analyzed. Peak 1–Peak 3 and Duration 1–Duration 3 correspond to the acceleration responses generated at the first, second, and third independent target plates, respectively. Therefore, separate regression equations were established for each acceleration characteristic. In this modeling framework, the differences among regression coefficients reflect the stage-dependent sensitivity of each acceleration characteristic to material mechanical properties. Thus, the coefficient variations are used to characterize the material–response relationships at different impact stages, while the overall

contribution of the target position in the impact sequence is evaluated separately through statistical analysis. The specific analysis is as follows:

- Influence on acceleration peaks (Peaks 1–Peaks 3);

For acceleration peaks, the regression models showed that elastic modulus, tensile yield strength, and compressive yield strength were positively correlated with peak acceleration, whereas dynamic compressive yield strength exhibited a negative coefficient within the present dataset. Mechanistically, elastic modulus, tensile yield strength, and compressive yield strength characterize the material's stiffness and resistance to deformation. Higher values of these parameters correspond to greater resistance to deformation under impact loading, leading to higher acceleration peaks. In contrast, the negative coefficient of dynamic compressive yield strength reflects the statistical relationship obtained from the current regression models. Under dynamic loading, a higher dynamic compressive yield strength usually indicates stronger resistance to plastic deformation before yielding occurs. Therefore, in this study, the negative coefficient should be understood as the result of the coupled influence of multiple material properties rather than as an isolated causal effect of dynamic compressive yield strength. This relationship may be associated with differences in material systems, stiffness, quasi-static strength, ductility, and dynamic deformation behavior among the tested alloys. The independent influence of dynamic compressive yield strength on peak acceleration still requires further verification using a larger material dataset.

- Influence on acceleration durations (Durations 1–3);

For acceleration durations, elastic modulus, elongation, and compressive yield strength showed positive coefficients, while ultimate tensile strength and dynamic compressive yield strength showed negative coefficients in the present regression models. The positive coefficients of elastic modulus and elongation indicate that higher stiffness and better ductility may extend the stress-wave interaction and deformation-buffering process during sequential impacts. In contrast, the negative coefficient of dynamic compressive yield strength suggests that, within the tested material range, materials with higher dynamic compressive yield strength tended to be associated with shorter pulse durations. This trend should also be interpreted as a coupled statistical relationship rather than a single-parameter causal mechanism, because pulse duration is affected by stress-wave propagation, local plastic deformation, local perforation, fracture, and the combined mechanical properties of the target material.

Differences exist in how parameters such as strength and elongation of the target material influence the acceleration of the impactor under sequential multiple-target impacts compared to single impacts. Wei et al. [23] employed an orthogonal experimental design to investigate the effects of density, elastic modulus, and strength of both the impactor and the target on acceleration parameters during a single impact, where the target underwent only elastic-plastic deformation without phenomena such as plugging. Their results indicated that the elastic modulus and quasi-static yield strength of the target significantly correlated with acceleration peaks and durations—both showing a positive correlation with peak acceleration but a negative correlation with duration. The findings of the present study partially align with those of Wei et al. [23], particularly in agreeing that the elastic modulus and quasi-static yield strength of the target material are positively correlated with peak acceleration. However, discrepancies arise regarding duration. The regression results of the present study indicate that the target material elastic modulus, compressive yield strength, and elongation are positively correlated with duration, whereas ultimate tensile strength and dynamic compressive yield strength show negative coefficients within the current dataset. This divergence may be attributed to differences in energy dissipation

mechanisms: in single non-penetrating impacts [23], energy is dissipated primarily through global deformation and rebound, where higher stiffness/strength shortens contact time. In contrast, under the sequential multiple-target impacts involving local perforation studied here, energy is dissipated through successive plastic deformation and local perforation and plastic deformation. Higher elastic modulus may prolong stress-wave interaction and residual vibration during successive impacts on independent target plates, thereby extending the acceleration duration. Meanwhile, the effect of dynamic compressive yield strength on duration may be coupled with other material properties, such as stiffness, ductility, and quasi-static strength, reflecting the combined influence of material deformation and failure behavior during sequential multiple-target impacts.

Based on the above analysis, a preliminary target-material selection strategy for sequential multiple-target impact experiments is summarized in Table 16. By selecting target materials with different mechanical properties, the acceleration peak and pulse duration generated during impact can be adjusted. Therefore, the proposed strategy can provide guidance for target material selection and for generating tunable overload responses in high-intensity impact testing of electromechanical components.

Table 16. Preliminary target-material selection strategy based on the current quantitative models.

Design Objective	Recommended Mechanical Property Profile	Representative Materials
High acceleration peak	Relatively high elastic modulus, tensile yield strength, and compressive yield strength	AISI 1020, AISI 1040
Long acceleration duration	Relatively high elastic modulus, elongation, and compressive yield strength	H62 brass
Balanced peak and duration	Relatively high elastic modulus, elongation, and compressive yield strength	S30153 stainless steel

Note: Dynamic compressive yield strength showed a negative coefficient in the current regression models. However, the negative coefficient is regarded as a coupled statistical effect within the present dataset rather than an independent material-selection criterion.

4.4. Future Research Directions

This study establishes a preliminary framework for correlating material properties with acceleration responses in sequential multiple-target impact tests. However, several limitations remain and should be addressed in future work. First, the present dataset includes only nine metallic materials. Therefore, future studies should expand the experimental database by incorporating a wider range of metal alloys, composite materials, and structural configurations. A larger dataset would allow more rigorous validation of the proposed models and improve their applicability to new material systems.

Second, the current models are based on linear and regularized linear regression methods. Although these models are suitable for the limited dataset and provide good interpretability, future work should explore nonlinear or hybrid modeling approaches when sufficient data are available. Such approaches may better capture complex relationships between material properties, target deformation, and acceleration characteristics.

Third, the present study focuses on sequential impacts on independent target plates, in which each target plate is impacted only once. Therefore, damage accumulation within the same target plate was not considered in the current model. Future studies may extend the framework to repeated impacts on the same target specimen or to more complex impact scenarios involving target damage evolution, impactor state evolution, support condition changes, work hardening, thermal softening, and other path-dependent effects.

Finally, mechanism-informed modeling approaches should be further developed. Physics-informed regression models, continuum-damage-based models, or hybrid models

combining mechanical theory with machine learning may provide more reliable predictions when extrapolating to new materials, geometries, or loading conditions.

These future developments will improve the predictive accuracy and engineering applicability of acceleration response models for structures subjected to sequential or repeated impact loading.

5. Conclusions

This study systematically investigated the effects of target material properties on acceleration characteristics during sequential multiple-target impacts through mechanical testing, sequential multiple-target impact experiments, and quantitative modeling. The main findings are summarized as follows:

- Material mechanical properties were identified as the dominant factors affecting acceleration responses under sequential multiple-target impacts ($p < 0.001$), and their influence was greater than that of the target position in the impact sequence in the present dataset;
- By comparing the fitting performance of regression models under different data-partitioning schemes, the optimal quantitative prediction models were selected. Ridge regression ($\alpha = 0.1$) was selected for Peak 1–Peak 3, Duration 1, and Duration 3, whereas linear regression was selected for Duration 2. Specifically, the partitioning scheme with six training samples and three test samples was adopted for Peak 1 and Peak 2, while the scheme with eight training samples and one test sample was applied for Peak 3 and Duration 1–Duration 3;
- Within the tested material range, the regression results showed statistical correlations between material mechanical properties and acceleration characteristics. For acceleration peaks, elastic modulus, tensile yield strength, and compressive yield strength were positively correlated with peak values, whereas dynamic compressive yield strength showed a negative coefficient in the present regression models. This negative coefficient may reflect the coupled effects of multiple material properties rather than the independent influence of dynamic compressive yield strength alone. For acceleration pulse widths, elastic modulus, elongation, and compressive yield strength were positively correlated with pulse duration, while ultimate tensile strength and dynamic compressive yield strength showed negative correlations. These relationships should be interpreted as statistical correlations within the current dataset rather than universal causal relationships;
- Based on the quantitative models, a preliminary target-material selection strategy was proposed. To obtain higher peak acceleration, materials with relatively high elastic modulus, tensile yield strength, and compressive yield strength, such as AISI 1020 and AISI 1040 steels, are preferred within the tested material range. To extend pulse duration, materials with relatively high elongation, such as H62 brass, may be selected. For balanced acceleration peak and duration characteristics, materials with a suitable combination of stiffness, strength, and ductility, such as S30153 stainless steel, may provide better overall performance.

These findings provide a preliminary predictive framework for analyzing the relationship between target material properties and acceleration characteristics under sequential multiple-target impact loading. From an engineering application perspective, the proposed models and target-material selection strategy can provide guidance for target material selection in sequential multiple-target impact experiments and offer an experimental approach for generating tunable overload responses in high-intensity impact testing of electromechanical components. However, because only nine metallic materials were tested, the proposed regression models are limited by the small sample size and potential overfitting

risk. Therefore, these models should be regarded as preliminary empirical prediction models within the tested material range rather than universally applicable models. Further validation using a larger material database and additional impact-test data is required before broader engineering application.

Supplementary Materials: The following supporting information can be downloaded at: https://www.mdpi.com/article/10.3390/app16115706/s1, Figure S1. Mechanical property test curves for different target materials: (**a**) Quasi-static tensile stress-strain curves; (**b**) Quasi-static compression stress-strain curves; (**c**) Dynamic compression stress-strain curves. Figure S2. Acceleration time-history curves obtained from sequential multiple-target impact experiments for different target materials: (**a**) AISI 1020 steel; (**b**) AISI 1040 steel; (**c**) AISI 1060 steel; (**d**) 2A12 Al alloy; (**e**) 7020 Al alloy; (**f**) 7075 Al alloy; (**g**) AZ31B Mg alloy; (**h**) H62 brass; (**i**) S30153 stainless steel.

Author Contributions: Conceptualization, H.S. and S.M.; methodology, H.S. and F.L.; software, H.S. and K.J.; validation, H.S. and K.J.; formal analysis, X.Z. and S.M.; investigation, H.S. and F.L.; data curation, H.S.; writing—original draft preparation, H.S.; writing—review and editing, S.M. and X.Z.; visualization, F.L.; supervision, S.M. All authors have read and agreed to the published version of the manuscript.

Funding: This research received no external funding.

Institutional Review Board Statement: Not applicable.

Informed Consent Statement: Not applicable.

Data Availability Statement: All data generated or analyzed during this study are included in the article. The data and intellectual property rights belong to Nanjing University of Science and Technology. The original contributions presented in this study are included in the article. Further inquiries regarding the data and intellectual property can be directed to the corresponding author.

Conflicts of Interest: The authors declare no conflicts of interest.

Nomenclature

Symbol/Abbreviation	Description	Unit/Note
PCB	Printed circuit board	—
SHPB	Split-Hopkinson pressure bar	—
AISI	American Iron and Steel Institute	—
SD	Standard deviation	—
ANOVA	Analysis of variance	—
Peak 1	Acceleration peak of the first impact	g
Peak 2	Acceleration peak of the second impact	g
Peak 3	Acceleration peak of the third impact	g
Duration 1	Pulse duration of the first impact	μs
Duration 2	Pulse duration of the second impact	μs
Duration 3	Pulse duration of the third impact	μs
x_1	Elastic modulus	GPa
x_2	Tensile yield strength	MPa
x_3	Ultimate tensile strength	MPa
x_4	Elongation percentage	%
x_5	Compressive yield strength	MPa
x_6	Dynamic compressive yield strength	MPa
y_{p1}	Acceleration peak of the first impact	g
y_{p2}	Acceleration peak of the second impact	g
y_{p3}	Acceleration peak of the third impact	g
y_{w1}	Pulse duration of the first impact	μs
y_{w2}	Pulse duration of the second impact	μs

y_{w3}	Pulse duration of the third impact	μs
p	Probability value	—
F	F-statistic	—
SS	Sum of squares	—
df	Degrees of freedom	—
MS	Mean square	—
F crit	F critical value	—
RMSE	Root mean square error	g or μs
MAPE	Mean absolute percentage error	%
MSE	Mean squared error	g^2 or ms^2
Z	Standardized value	—
z	Original value	—
$\bar{z}$	Mean	—
s_z	Standard deviation of the variable	—
y_i	Measured value of the output Variable of the *i*-th sample	g or μs
$\hat{y}_i$	Predicted value of the output Variable of the *i*-th sample	g or μs
y	Vector of measured output Variables	g or μs
b	Bias term/intercept of the regression model	g or μs
x_j	The *j*-th standardized input Variable	—
x_{ij}	The *j*-th standardized input Variable of the *i*-th sample	—
X	Input matrix composed of standardized input Variables	—
ω	Regression coefficient vector	—
ω_j	Regression coefficient of the *j*-th input Variable	—
m	Number of training samples	—
n	Number of input Variables	—
$L_{L2}(\omega)$	Loss function with L2 regularization	—
$L_{L1}(\omega)$	Loss function with L1 regularization	—
$L_{MSE}(\omega)$	Loss function of the regression model	—
$L(\omega)$	Loss function of the Elastic Net model	—
α	Regularization strength parameter	—
l_1	Mixing parameter of Rlastic Net	$0 \leq l_1 \leq 1$

References

1. Johnson, A.A.; Storey, R.J. The impact fatigue properties of iron and steel. *J. Sound Vib.* **2007**, *308*, 458–466. [CrossRef]
2. Taushanov, A.; Spasova, E. Determination of vehicle impact loads according to different design codes. *Annu. Univercity Archit. Civ. Eng. Geod.* **2024**, *57*, 739. [CrossRef]
3. Wang, T.X.; Dong, Z.J.; Cao, C.; Zhou, J.; Meng, Y.H.; Quan, W.W. Characterization of aircraft landing impact loads: Effects on vertical tire-pavement contact characteristics and pavement performance. *Constr. Build. Mater.* **2024**, *457*, 139365. [CrossRef]
4. Liu, P.; Li, J.; Li, C.S.; Li, H.J.; Zhang, J.M.; Zhang, H. Analysis of the influence of different initial velocities on dynamic performance of multi-layer hard target penetration process. *Front. Phys.* **2023**, *11*, 1241762. [CrossRef]
5. Sangid, M.D. The physics of fatigue crack propagation. *Int. J. Fatigue* **2025**, *197*, 108928. [CrossRef]
6. Zhao, S.H.; Li, B.L.; Yuan, K.B.; Guo, W.G.; Li, P.H.; Wang, R.F.; Yang, J.H.; Gao, M. Design of a continuously repeated impact method with constant amplitude based on Hopkinson bar: Principle and impact fatigue life testing. *Int. J. Impact Eng.* **2024**, *193*, 105038. [CrossRef]
7. Wagner, U.; Muller-Fiedler, R.; Bagdahn, J.; Michel, B.; Paul, O. Mechanical reliability of epipoly MEMS structures under shock load. In *Proceedings of the TRANSDUCERS '03. 12th International Conference on Solid-State Sensors, Actuators and Microsystems, Boston, MA, USA, 8–12 June 2003*; Digest of Technical Papers (Cat. No.03TH8664); IEEE: Piscataway, NJ, USA, 2003; Volume 171, pp. 175–178.
8. Srikar, V.T.; Senturia, S.D. The reliability of microelectromechanical systems (MEMS) in shock environments. *J. Microelectromechanical Syst.* **2002**, *11*, 206–214. [CrossRef]
9. Wang, J.J.; Song, Y.C.; Wang, W.; Li, J. Calibrations of numerical models by experimental impact tests using scaled steel boxes. *Eng. Struct.* **2018**, *173*, 481–494. [CrossRef]

10. Ma, X.; Zhang, S.R.; Tang, T.; Yu, D.; Wang, X.F.; Zhang, H.; Ding, L.B.; Dai, K.R. A Lightweight High-Impact Acceleration State Reconstruction Method for Multibody Dynamic Systems by an Extended Kalman Filter-Aided Time Neural Network. *IEEE Sens. J.* **2024**, *24*, 31524–31537. [CrossRef]
11. Chen, X.D.; Xu, L.Y.; Zhu, Q. Mechanical behavior and damage evolution for concrete subjected to multiple impact loading. *KSCE J. Civ. Eng.* **2017**, *21*, 2351–2359. [CrossRef]
12. Yang, Y.C.; Li, Q.W.; Qiao, L. Review of SHPB Dynamic Load Impact Test Characteristics and Energy Analysis Methods. *Processes* **2023**, *11*, 3029. [CrossRef]
13. Shi, H.F.; Tang, T.; Li, J.Y.; Li, F.Y.; Ma, S.J.; Zhang, X.P. Low-velocity, high-energy impact methodology for simulating overload responses during multilayer projectile penetration. *Results Eng.* **2026**, *29*, 109042. [CrossRef]
14. Zhang, W.G.; Wu, C.Z.; Li, Y.Q.; Wang, L.; Samui, P. Assessment of pile drivability using random forest regression and multivariate adaptive regression splines. *Georisk Assess. Manag. Risk Eng. Syst. Geohazards* **2021**, *15*, 27–40. [CrossRef]
15. Li, J.C.; Cheng, G.; Lu, Y.G.; Huang, F.L. Investigation on the application of Taylor impact test to high-G loading. *Front. Mater.* **2021**, *8*, 717122. [CrossRef]
16. Sun, J.M.; Chen, H.; Yi, F.; Ding, Y.B.; Zhou, Y.; He, Q.F.; Zhang, W.X.; Yi, W.J. Experimental and numerical study on influence of impact mass and velocity on failure mode of RC columns under lateral impact. *Eng. Struct.* **2024**, *314*, 118416. [CrossRef]
17. Si, S.P.; He, C.; Liu, S.; Fan, B.J.; Xie, R.Y.; Xue, X.Y.; Liu, J.X. Influence of impact velocity on impact-initiated reaction behavior of Zr-Ti-Nb alloy. *Mater. Des.* **2022**, *220*, 110846. [CrossRef]
18. Huang, G.Y.; Feng, S.S.; Wu, G.; Li, S.P. Performance of different projectile nose shapes in normal penetrating armor targets. *Adv. Mater. Res.* **2011**, *308–310*, 1420–1425. [CrossRef]
19. Deng, J.J.; Zhang, X.F.; Liu, C.; Wang, W.J. Penetration performance of axisymmetric U-shape-nose grooved projectile into aluminum target: Theoretical model and experiment. *Lat. Am. J. Solids Struct.* **2018**, *15*, e46. [CrossRef]
20. Li, J.C.; Chen, G.; Huang, F.L.; Lu, Y.G. Load characteristics in Taylor impact test on projectiles with various nose shapes. *Metals* **2021**, *11*, 713. [CrossRef]
21. Xu, X.N.; Liu, Y.; Zhao, M.H.; Wu, C.F.; Pei, Y.H.; Zhang, C.M. Discrete-continuous coupling simulation and experimental research on peak impact acceleration in falling weight-layered system collisions. *Int. J. Impact Eng.* **2025**, *204*, 105374. [CrossRef]
22. Wang, G.B.; Mei, H.; Yin, Y.; Wang, J.N.; He, W.; Zhai, Y.X. Reduction coefficient investigation of strong ground surface impact load models considering energy loss. *J. Vib. Eng.* **2025**, *38*, 909–918. (In Chinese) [CrossRef]
23. Wei, J.; Ma, S.J.; Li, F.Y.; Dong, X.H.; Zhang, X.P. Influence of material properties and geometric parameters of an impact pair on contact acceleration during a low-velocity impact. *Mater. Today Commun.* **2021**, *29*, 102811. [CrossRef]
24. Bijalwan, P.; Senthil, K. Influence of steel slag as partial replacement of coarse aggregate in the fibre reinforced concrete curved beam under static and impact load. *Structures* **2024**, *67*, 106926. [CrossRef]
25. Liu, C.; Zhang, X.F.; Huang, C.Q.; Ding, L.; Chen, H.H.; Wang, J.P. Analysis of dynamic resistance and dynamic hardness test of metal target material. *J. Natl. Univ. Def. Technol.* **2020**, *42*, 162–169. [CrossRef]
26. Chao, H.X.; Lei, Q.; Du, W.B.; Ding, G.; Li, B.; Feng, J.W. Simulation and experimental investigation of high-speed projectile impacting closed-cell aluminum foam. *Vibroengineering Procedia* **2018**, *20*, 185–190. [CrossRef]
27. Cai, W.; Li, S.X.; Zhu, L.; Cao, D.F.; Guo, K.L.; Li, Y.G. A systematic review on dynamic responses of marine structures under repeated mass impacts. *Ocean Eng.* **2024**, *294*, 116790. [CrossRef]
28. Atoui, O.; Maazoun, A.; Aminou, A.; Belkassem, B.; Pyl, L.; Lecompte, D. Dynamic Behavior of Aluminum Plates Subjected to Sequential Fragment Impact and Blast Loading: An Experimental Study. *Appl. Sci.* **2023**, *13*, 3542. [CrossRef]
29. *GB/T 7314-2017*; Metallic Materials—Compression Test Method at Room Temperature. Standards Press of China: Beijing, China, 2017.
30. *GB/T 228.1-2021*; Metallic Materials—Tensile Testing—Part 1: Method of Test at Room Temperature. Standards Press of China: Beijing, China, 2021.
31. Tang, T.; Shi, H.F.; Li, F.Y.; Ma, S.J.; Zhou, J.L.; Liang, S.S.; Zhang, X.P. Modeling the mechanical properties of an impacted body and the overload signal characteristic parameters of the projectile during the impact. *Sci. Rep.* **2025**, *15*, 8095. [CrossRef] [PubMed]